Front. Earth Sci. 2018, 12(4): 765–778
https://doi.org/10.1007/s11707-018-0736-6

RESEARCH ARTICLE

Development of the DayCent-Photo model and integration of variable photosynthetic capacity

Jonathan R. STRAUBE (✉)[1,2], Maosi CHEN[1], William J. PARTON[1,2], Shinichi ASSO[1,2], Yan-An LIU (✉)[3,4,5,1], Dennis S. OJIMA[2], Wei GAO[1,6,5]

1 USDA UV-B Monitoring and Research Program, Natural Resource Ecology Laboratory, Colorado State University, Fort Collins, CO 80521, USA
2 Natural Resource Ecology Laboratory, Colorado State University, Fort Collins, CO 80523, USA
3 Key Laboratory of Geographic Information Science (Ministry of Education), East China Normal University, Shanghai 200241, China
4 School of Geographic Sciences, East China Normal University, Shanghai 200241, China
5 ECNU-CSU Joint Research Institute for New Energy and the Environment, Shanghai 200062, China
6 Department of Ecosystem Science and Sustainability, Colorado State University, Fort Collins, CO 80523, USA

Abstract We integrated a photosynthetic sub-model into the daily Century model (DayCent) to improve the estimations of seasonal changes in carbon fluxes at the Niwot Ridge LTER site and the Harvard forest LTER site (DayCent-Photo). The photosynthetic sub-model, adapted from the SIPNET/PnET family of models, includes solar radiation and vapor pressure deficit controls on production, as well as temperature and water stress terms. A key feature we added to the base photosynthetic equations is the addition of a variable maximum net photosynthetic rate (*Amax*). We optimized the parameters controlling photosynthesis using a variation of the Metropolis-Hastings algorithm along with data-assimilation techniques. The model was optimized and validated against observed net ecosystem exchange (NEE) and estimated gross primary production (GPP) and ecosystem respiration (RESP) values for AmeriFlux sites at Niwot Ridge and Harvard forest. The inclusion of a variable *Amax* rate greatly improved model performance (NEE RMSE = 0.63 $gC \cdot m^{-2}$, AIC = 2099) versus a version with a single *Amax* parameter (NEE RMSE = 0.74 $gC \cdot m^{-2}$, AIC = 3724). DayCent-Photo was able to capture the inter-annual and seasonal flux patterns for NEE, GPP, ecosystem respiration (RESP), and daily actual evapotranspiration (AET), but tended to overestimate yearly NEE uptake. The DayCent-Photo model has been successfully set up to simulate daily NEE, GPP, RESP, and AET for deciduous forest, conifer forests, and grassland systems in the US using AmeriFlux data sets and has recently been improved to include the impact of UV radiation surface litter decay (DayCent-UV). The simulated influence of a variable *Amax* rate suggests a need for further studies on the process controls affecting the seasonal photosynthetic rates. The results for all of the forest and grassland sites show that maximum *Amax* values occurs early during the growing period and taper off toward the end of the growing season.

Keywords DayCent-Photo model, seasonal maximum net photosynthetic rate, net ecosystem exchange, gross primary production, UV radiation

1 Introduction

Forest ecosystems exchange vast amounts of CO_2 to and from the atmosphere (Schimel, 1995), serving as a net sink (Luyssaert et al., 2008, 2010), and playing an important role in curbing the increase of atmospheric CO_2 concentrations. In forest ecosystems, the net exchange of carbon between atmosphere and live biomass is strongly regulated by the seasonality of photosynthesis (Huxman et al., 2003; Monson et al., 2005). However, the seasonality is poorly represented in terrestrial biosphere models (Sacks et al., 2006; Richardson et al., 2013). The AmeriFlux net carbon exchange studies provide a data set to measure and understand the factors affecting net ecosystem exchange (NEE) in different biomes across the globe. This study utilizes the long term forest ecosystem observations of the Niwot Ridge AmeriFlux site to explore the role of variable photosynthetic rates on seasonal carbon exchange for conifer systems and shows how variable maximum photosynthesis rates impact ecosystem dynamics for

Received June 12, 2018; accepted September 5, 2018

E-mails: jonathan.straube@colostate.edu (Jonathan R. STRAUBE), yaliu@geo.ecnu.edu.cn (Yan-An LIU)

deciduous forest and grassland systems using the photosynthetic version of the DayCent ecosystem model (DayCent-Photo) (Savage et al., 2013).

The seasonality of photosynthesis results from changes in photosynthetic capacity, and affects gross primary production (GPP) and ultimately net ecosystem exchange. Aspects including the variation of stem xylem hydraulic conductivity, enzyme activity, mesophyll conductance, stomatal conductance, electron transport efficiency, quantum efficiency, and general leaf design principles have been found to relate to the seasonal dynamics of photosynthesis (Granda et al., 2014; Urban et al., 2017; Zhang et al., 2017; Martinez and Fridley, 2018). The seasonal changes in photosynthetic capacity are well-documented in forest systems (Bourdeau, 1959; Helms, 1965; Mohren and van de Veen, 1995; Marshall et al., 2001; Huxman et al., 2003; Wang and Barrett, 2003; McGarvey et al., 2004; Weiskittel et al., 2006). In an evergreen forest, photosynthetic capacity increases rapidly in the spring warm up, allowing the forest to assimilate a large portion of GPP for the year during the early snow melt period (Monson et al., 2005). Photosynthetic capacity then generally declines in the dry or cool season in most (woody) species (Zhang et al., 2014, 2017). The seasonality of photosynthesis varies among species. Guan et al. (2014) found that the net photosynthetic rate peaked in summer for two species (*Pinus massoniana* and *Castanopsis sclerophylla*) but in autumn for two other species (*Lithocarpus glaber* and *Cyclobalanopsis glauca*). Urban et al. (2017) found that photosynthetic capacity peaked in August and September for Norway spruce (i.e., *Picea abies*). Li et al. (2018) reported that for *Ammopiptanthus mongolicus*, photosynthetic capacity increased from January, reached the highest value in July, and greatly declined in September. Martinez and Fridley (2018) found that photosynthetic capacity peaked in spring and declined through summer and autumn for common species in central New York (i.e., *Acer negundo*, *Liriodendron tulipifera*, *Acer saccharum*, *Tsuga Canadensis*, and *Pinus strobus*). The seasonality of photosynthesis and other ecological processes is usually examined with short-term experiments or observations at small plots, and projecting to larger temporal and spatial scales involves mathematical models such as the DayCent model (Rastetter et al., 2003). Incorporating the seasonality of photosynthetic capacity to terrestrial biosphere models will allow the models to better simulate the inter-annual dynamics in NEE and improve carbon flux estimates at the seasonal and annual level (Wang et al., 2007; Tang et al., 2013).

The original version of the DayCent model (Parton et al., 2001) was developed to model soil trace gas fluxes such as N_2O, NO_x, CH_4, and CO_2, and plant production for forest, cropland, grassland, and savanna ecosystems. A version specific to forests was developed to better represent the ecosystem dynamics for forest systems (ForCent) (Parton et al., 2010). All DayCent versions include complex controls of soil nutrients, soil water and temperature, and atmospheric CO_2 levels on plant growth (Parton et al., 2010). The DayCent model have been used to simulate long-term ecological processes at forest sites such as the Harvard Forest site in Massachusetts and the Niwot Ridge site in Colorado. Frey et al. (2013) used the DayCent model to simulate the effects of soil warming on soil C storage at the Harvard forest site in response to altering the microbial efficiency parameter in the model. Savage et al. (2013) used the DayCent model to simulate the long-term impacts of warming and N deposition on the distribution of forest C stocks at the Harvard forest site. Hartman et al. (2014) used the DayCent model to investigate the combined effects of climate, atmospheric N deposition, and CO_2 on many ecosystem variables at seven forested montane including the Niwot Ridge site.

The DayCent model was updated to include a photosynthetic sub-model from the Simple Photosynthesis and Evapotranspiration (SIPNET) model (Braswell et al., 2005; Sacks et al., 2006) to better simulate ecosystem dynamics (Savage et al., 2013), and modified to incorporate the seasonally variable photosynthetic capacity in the calculation of GPP (DayCent-Photo). This paper will present a detailed description of the DayCent-Photo model and its validation against eddy covariance data collected at Niwot Ridge AmeriFlux site. DayCent-Photo has recently been revised to include the impact of ultraviolet-B (UV-B) radiation on grassland and forest ecosystems (DayCent-UV) and has been successfully used to simulate ecosystem dynamics for the short grass steppe ecosystem in Eastern Colorado (Chen et al., 2016, 2017). The data collected at the Niwot Ridge LTER high-altitude forest site include extended series of carbon and water flux measurements, and have been successfully used with model-data fusion techniques to provide well constrained estimates of system level fluxes (Braswell et al., 2005; Sacks et al., 2006, 2007; Moore et al., 2008; Zobitz et al., 2008). We parameterized DayCent-Photo with a model-data synthesis technique that is a variation of the Markov Chain Monte Carlo (MCMC) algorithm, and evaluated model performance with a combined likelihood given daily fluxes observed at the Niwot Ridge site. We will compare two version of the model, one with variable maximum photosynthetic capacity (*Amax*), and one with a fixed *Amax*. Since we don't have a variable *Amax* function, optimizing the parameters controlling photosynthesis, using model-data fusion techniques, will create a synthetic stand-in for that function. We will then do a model comparison to see if variable *Amax* could be a significant factor in control production.

2 Methods

Here we describe the DayCent-Photo model which includes the SIPNET photosynthesis model, the NIWOT

ridge high elevation conifer site, the eddy covariance data used to calibrate and test the model performance, and the procedure used to determine the optimal parameters for the SIPNET sub-model. We used the observed daily value of NEE, GPP, and actual evapotranspiration (AET) from the eddy covariance site at NIWOT ridge to calibrate and test the model.

2.1 Niwot Ridge site and data description

Data used were from the Niwot Ridge AmeriFlux site (US-NR2) (40.0329°N Latitude; 105.5464°W Longitude), a high-elevation (3030 m), subalpine forest on the western side of the Continental Divide. The site is a part of the Roosevelt National Forest, approximately 50 miles west of Boulder, Colorado in the Rocky Mountain Range, with mean annual temperature of 4°C and mean annual precipitation of 800 mm of which ~65% falling as snow (Monson et al., 2002). The dominant tree species in this area are subalpine fir (*Abies lasiocarpa*), Engelmann spruce (*Picea engelmannii*), and lodgepole pine (*Pinus contorta*). The forest stand at the site is approximately 100 years old and is a natural secondary growth, established following clear-cut logging from 1900 to 1910. The site's understory is sparse, with 25% average cover, and is composed of seedlings, Whortleberry (*Vaccinium myrtillus* L.), moss, and lichens. The soil at the site is sandy due to rocky granite composition, with a surface layer of ~6 cm of organic material. Estimates for above ground biomass of carbon range from 11,500 to 24,000 $gC \cdot m^{-2}$ (Blanken et al., 2010), and the site is a carbon sink with a cumulative annual rate ranging from 60 – 80 $gC \cdot m^{-2}$ (Monson et al., 2002; Tang et al., 2012).

The data at the site were collected by eddy covariance method (Baldocchi et al., 1988; Baldocchi, 2003) and retrieved from the AmeriFlux website (Blanken et al., 2010). Briefly, the eddy covariance method measured CO_2 concentration above the canopy with a sonic anemometer and an infrared gas analyzer, converted the raw data to half hourly fluxes of NEE applying various correction measures. The data were gap-filled using the Marginal Distribution Sampling method (Papale and Valentini, 2003; Reichstein et al., 2005) and u-star filtered, to account for periods of low turbulence in the air mass that affect flux calibrations. Estimates for ecosystem respiration (RESP) were calculated by the short-term temperature response of nighttime NEE fluxes (Reichstein et al., 2005), and GPP estimates were calculated as GPP = RESP – NEE. The data were in half hour flux rates, and were aggregated into daily values. A detailed description of data collection is available elsewhere (Monson et al., 2002; Turnipseed et al., 2002, 2003, 2004). The climate variables were air temperature, precipitation, global radiation, and vapor pressure deficit while the flux variables included GPP, NEE, RESP, and AET.

2.2 Model structure

The DayCent-Photo model is an ecosystem model (Fig. 1) capable of simulating plant growth, soil carbon processes, daily NEE, GPP, and AET fluxes, soil nutrient cycling (N, P, S, and K) and trace gas fluxes (N_2O, NO_x, N_2, and CH_4), and is set up to simulate the impact of management practices on natural and managed grasslands, forests, cropland, and savannas ecosystems (Parton et al., 1998, 2001; Del Grosso et al., 2000). Plant growth is simulated through the processes of assimilation, allocation of carbon to different plant parts, and exchange of water, carbon and other nutrients. The processes occur in various compartments of the system, with each compartment representing a different plant and soil functions (roots, wood, leaves, litter layer, soil, etc.) The earlier version of the ForCent model (Parton et al., 2010) estimates GPP as a scalar value twice that of the calculated NPP, and NPP in turn is a function of genetic potential, soil temperature, available water, solar radiation, and available nutrients (Parton et al., 2010).

The DayCent-Photo model uses the SIPNET with simplified Farquar photosynthesis to calculate daily GPP as a function of maximum photosynthetic assimilation rate (GPP_{max}) that is the unstressed (not including climatic factors) net instantaneous CO_2 assimilation rate per unit leaf mass:

$$GPP_{max} = Amax*(AmaxFrac + BaseFolRespFrac), \quad (1)$$

where *Amax* is the maximum net CO_2 assimilation rate per unit leaf mass, *AmaxFrac* is the average daily maximum photosynthesis as a fraction of *Amax*, and *BaseFolRespFrac* is the foliar respiration as a fraction of *Amax*.

The GPP_{max} value is then scaled by the four terms that represent climatic conditions with values between zero and one: temperature (D_{temp}), vapor pressure deficit (D_{vpd}), solar radiation (D_{light}), and a water stress term (D_{water}) such that

$$GPP = GPP_{max}*D_{temp}*D_{light}*D_{water}. \quad (2)$$

This equation is from the SIPNET model (Monson et al., 2002; Braswell et al., 2005; Sacks et al., 2006, 2007) and the SIPNET model is based on the PnET model (Aber and Federer, 1992) designed to be used with eddy covariance data in a model-data fusion approach for estimating parameter values. Further descriptions and equations for these scaling terms can be found in Braswell et al. (2005). We modified the calculation for D_{vpd} to improve the effect of stomatal conductance due to lack of air moisture (VPD). The values for D_{vpd} is calculated as an exponential decline in efficiency (Drake et al., 2010):

$$D_{vpd} = DVPDSlope*e^{DVPDExp*VPD}, \quad (3)$$

where *DVPDExp* and *DVPDSlope* are the shape parameters controlling the VPD photosynthesis relationship.

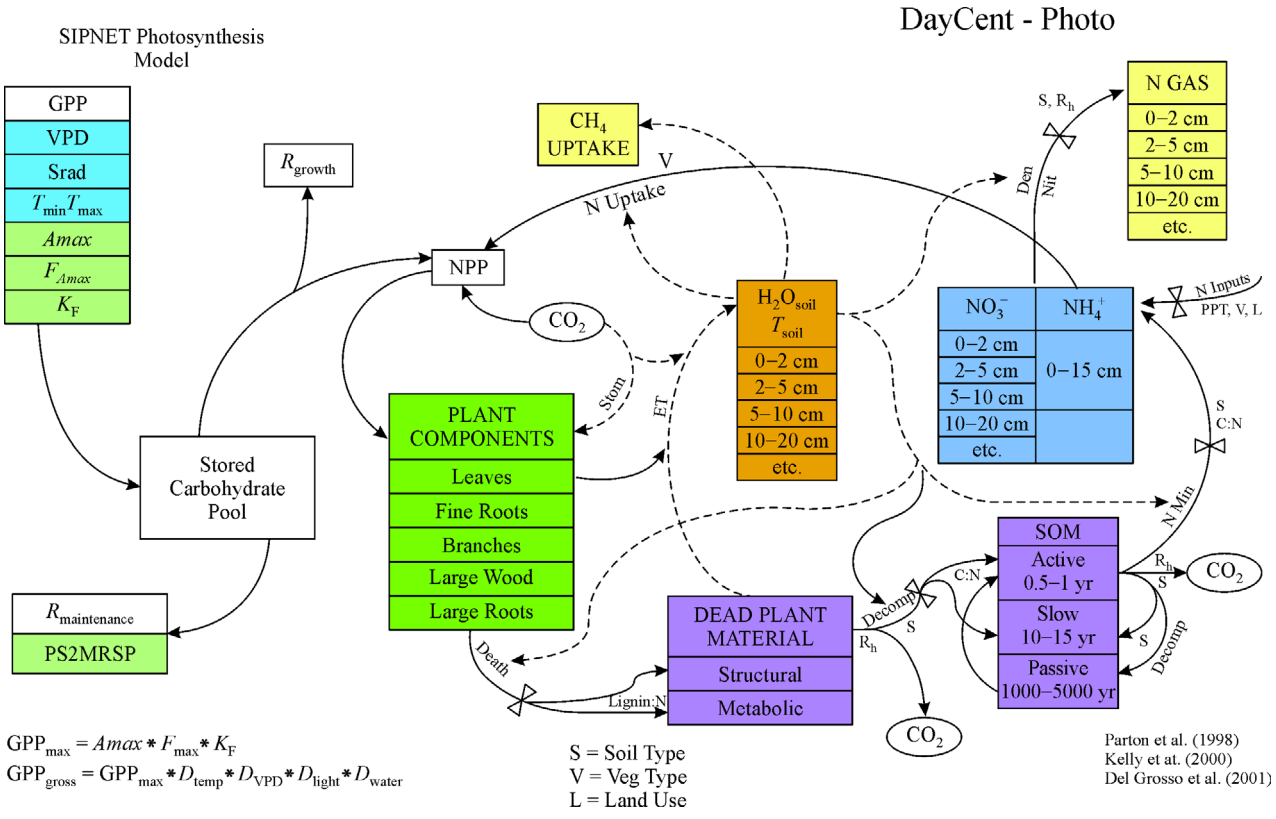

Fig. 1 The DayCent model with the photosynthetic modifications. Maintenance respiration is based on the PS2Mrsp parameter.

The original version of the SIPNET model included a single *Amax* throughout all seasons. We changed the SIPNET model so that seasonal changes in *Amax* are represented using a linear *Amax* response function as observed by Marshall et al. (2001) in Douglas-fir, Ponderosa pine, and Western white pine of northern Idaho. The response function scales the value of *Amax* from the start of one growth period to the end of the growing period (Fig. 2) as defined by the GrowthDays parameters (the number of days since the start of the growing season). The function allows the *Amax* value to be scaled three times during the growing season. Figure 2 shows the seasonal changes in the *Amax* scalar derived from the model optimization process. The figure also shows the seasonal changes in the *Amax* scalar for the Harvard forest site, and the SGS short grass steppe site (Savage et al., 2013; Chen et al., 2017). The optimal values for the Harvard forest and SGS sites were determined using eddy covariance data sets.

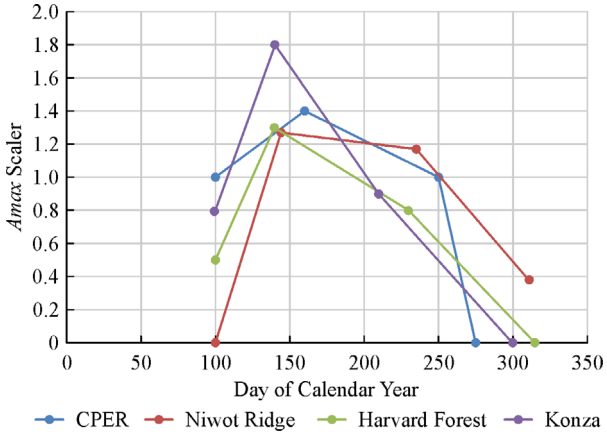

Fig. 2 The optimized seasonal values of *Amax* at Niwot Ridge, CPER, Harvard Forest, and Konza sites.

2.3 Statistical analysis and parameter optimization

We used an optimization technique to estimate the parameter values for both the SIPNET photosynthesis routine and for the variable *Amax* function, optimized against observations of GPP and NEE. The additional use of GPP and NEE for optimization greatly improves the model results for all flux estimates and keeps the parameters controlling photosynthesis from over-fitting the data and exceeding the literature-defined parameter boundaries. We chose not to use AET as an optimization parameter because changes in photosynthetic parameters do not affect the value of AET in our version of the photosynthetic sub-model. The parameter optimization scheme used is a variation of the Metropolis-Hastings algorithm, with a simulated annealing algorithm (Hurtt and

Armstrong, 1996) to help prevent parameter values from settling into local optima. The algorithm performs a quasi-random walk through the parameter space, via the Metropolis-Hastings algorithm, to find a parameter set that minimizes model error and maximizes the likelihood function (L) (Braswell et al., 2005; Sacks et al., 2006, 2007; Moore et al., 2008). The algorithm produces a maximum likelihood estimation (MLE), which is the parameter vector that most strongly supports the data (Fisher, 1932).

This model optimization method based on maximum likelihood estimation allows for several candidate models (or model parameterizations in this case) to be evaluated and ranked based on the support by the data (Johnson and Omland, 2004). The likelihood function compares model hypothesis by calculating confidence bounds of parameters, which we cannot do with sum of squares (Hilborn and Mangel, 1997).

We sum the calculated probabilities for multiple parameters by using log-likelihood for a total likelihood or *Ltotal*. By convention we are using a negative log-likelihood, as seen in the following equation, since we are maximizing the likelihood function. Future references to log-likelihood should be considered a negative log-likelihood. The best parameter set produces a result that maximizes log-likelihood which is computed as

$$l = [n \log \sigma] - \left[\frac{1}{2\sigma^2}\Sigma_{i=1}^{n}(x_i - \mu_i)^2\right], \quad (4)$$

where n is the number of observations, σ is the standard deviation for the data, x_i is an observed data point, and μ_i is the corresponding modeled point. This form of the log-likelihood equation is easy to work with because the number of observations n and the sum of squares of the residuals is readily available, and the standard deviation can be estimated from the sum of squares. Constants that do not affect the likelihood comparison were removed from the equation. Standard deviation, σ, was estimated because the actual error for NEE and GPP data is unknown. We estimated the standard deviation, σ_e, according to the method in Braswell et al. (2005):

$$\sigma_e = \sqrt{\frac{1}{n}\Sigma_{i=1}^{n}(x_i - \mu_i)^2}. \quad (5)$$

The optimization process proceeds in iterative sequences. For each run (a 2000 years' simulation), the optimization process randomly selects a parameter, changes it by a random amount, and compares the resulting model output against observed NEE and estimated GPP data. If the new candidate parameter set increases log-likelihood, that set is then accepted. If the new candidate set does not have an improved likelihood, it may still be accepted with a probability equal to the difference of the log-likelihoods from the old to the new parameter sets to ensure that the global optimum is found. The likelihood calculation is an iterative Bayesian calculation sampled from a posterior distribution of the model error that is assumed to have a Gaussian probability distribution. After an adequate number of runs, the sampled space should represent the posterior probability distribution of parameters, and the Metropolis-Hastings algorithm guarantees convergence to a stationary point in the parameter space. Parameter ranges and initial starting values that are directly equivalent to the parameters of the SIPNET model are used from the previous work of Moore et al. (2008), see Table 1. A near optimal parameter set, suitable for a model comparison, was retrieved with the methodology set forth in this paper. Extensive plant production, soil carbon and nitrogen, and biomass data from the Niwot Ridge LTER site (http://niwot.colorado.edu/) were used to calibrate the ability of the model to correctly simulate observed soil carbon and nitrogen, plant production and live plant biomass (Del Grosso et al., 2008) levels for the Niwot Ridge site. R^2 and Root Mean Squared Error (RMSE) were used as the statistical method to validate the results. R^2 measures the proportion of variability in Y explained by the regression model. It is the square of the correlation r. RMSE measures the standard deviation of the residuals (the spread of the points about the fitted regression line).

3 Results

3.1 Optimization of photosynthesis parameters

We compared the Moore et al. (2008) best parameter estimates for the SIPNET photosynthesis model (Table 1) with the optimum SIPNET photosynthesis parameters in DayCent-Photo for the single and variable *Amax* runs (Table 2). As expected, these were significantly different from the original starting parameter used from Moore et al. (2008). We expected to see differences in the parameterizations because the DayCent-Photo was optimized on two carbon flux values (NEE and GPP), whereas the SIPNET model was optimized on NEE and AET. Values of the best parameterizations fell well within the allowable range for each parameter for both DayCent-Photo variable *Amax* and single *Amax* versions and were generally quite similar for both versions of the model. Figure 2 shows the seasonal changes in the *Amax* scalar derived from the optimization of the photosynthesis parameters for the Niwot ridge site and three other sites from previous studies (Savage et al., 2013; Chen et al., 2016, 2017). The seasonal pattern of the *Amax* scalar was similar among DayCent-Photo (or DayCent-UV) adjusted for Niwot Ridge, Harvard forest (Savage et al., 2013), short grass steppe of Colorado (CPER) (Chen et al., 2016, 2017), and tall grass prairie at Konza Biological Station in northern Kansas. The results

Table 1 Photosynthetic parameters, starting values and ranges. Parameters marked with an (*) are taken from Moore et al. (2008). Values marked with a (#) are from Sarah Davis, personal communication. Estimates for PS2Mrsp are taken from literature values for maintenance respiration (Ryan and Waring, 1992). Fixed parameters do not change during the optimization process. Parameters are considered to have no units unless labeled otherwise

Parameter	Description	Range	Starting value
+ PS2Mrsp	Fraction of GPP applied to maintenance respiration	0.3 to 0.65	0.46
**Amax*	Maximum net CO_2 assimilation rate	0 to 34	4.9 ($gC \cdot m^{-2}$)
**AmaxFrac*	Ave. daily max photosynthesis as a fraction of *Amax*	fixed	0.76
*AmaxScalar*1	Scalar value of *Amax* at *GrowthDays*1	fixed	0
*AmaxScalar*2	Scalar value of *Amax* at *GrowthDays*2	0.8 to 1.6	1.22
*AmaxScalar*3	Scalar value of *Amax* at *GrowthDays*3	0.7 to 1.5	1.03
*AmaxScalar*4	Scalar value of *Amax* at *GrowthDays*4	0.3 to 0.8	0.6
**Attenuation*	Canopy Par extinction coefficient	fixed	0.5
**BaseFolRespFrac*	Foliar respiration as a fraction of *Amax*	0.05 to 0.3	0.06
**CFracLeaf*	Fraction of carbon applied to leaf growth	0.2 to 1	0.52
#*DVPDExp*	Exponent of VPD-photosynthesis relationship	fixed	−0.35
#*DVPDSlope*	Slope of VPD-photosynthesis relationship	fixed	1.55 (kPa^{-1})
*GrowthDays*1	First day of growth to apply *AmaxScalar*1 scalar	fixed	1 (day)
*GrowthDays*2	Number of days after the start of growth to apply *AmaxScalar*2 scalar	20 to 120	42 (days)
*GrowthDays*3	Number of days after the start of growth to apply *AmaxScalar*3 scalar	121 to 180	136 (days)
*GrowthDays*4	Number of days after the start of growth to apply *AmaxScalar*4 scalar	181 to 220	209 (days)
**HalfSatPAR*	Half saturation point of PPFD-photosynthesis relationship	4 to 12	8.3 ($mol \cdot m^{-2} \cdot d^{-1}$)
**LeafCSPWT*	Carbon content of needles on a per-area basis	fixed	270
**PsntMin*	Minimum temperature for photosynthesis	−8 to 8	−3.5 (°C)
**PsntOpt*	Optimum temperature for photosynthesis	5 to 30	18.9 (°C)

show a rapid increase in the *Amax* scalar during the spring (April 1 to May 30), slow decrease during the summer, and a rapid decrease at the end of the growing season.

3.2 Simulation of observed seasonal patterns

Variable *Amax* improved the ability of DayCent-Photo to simulate observed seasonal patterns in NEE and GPP at Niwot Ridge (Table 3). Variable *Amax* was favored over single *Amax* by all statistical indices used (Table 3). DayCent-Photo with variable *Amax* had substantially lower RMSE for both NEE and GPP with the variable *Amax* version (0.63 vs. 0.74 $gC \cdot m^{-2}$ for NEE and 0.88 vs. 1.02 $gC \cdot m^{-2}$ for GPP) while the higher R^2 values for NEE and GPP. The AIC value for the variable *Amax* model (2099.0) was significantly better than for the single *Amax* model (3723.9) (Table 3).

With variable *Amax*, DayCent-Photo simulated the phenology of NEE and GPP reasonably well at the Niwot Ridge site, whereas the single *Amax* version greatly underestimated the spring uptake (Fig. 3). The comparison of observed and simulated mean weekly NEE showed a strong carbon uptake (downward pattern) during the early spring snow melt (weeks 16 to 20-May) for the observed NEE, followed by a reduction of the uptake in mid-summer as heterotrophic respiration increase, and another smaller increase in the latter summer period that coincides with summer monsoonal moisture common in this study area. Examination of NEE residuals between weeks 13 − 25 showed over twice the cumulative error for the single *Amax* model (7.6 $gC \cdot m^{-2}$) compared to the variable *Amax* version (3.4 $gC \cdot m^{-2}$). Residual errors for the remainder of the growing season on were similar at 2.5 and 2.9 $gC \cdot m^{-2}$, respectively. The observations for GPP (Fig. 3(b)) showed a rapid increase during the spring (weeks 14 to 20), a gradual decline during the summer, and a rapid decline in the fall. The variable *Amax* version again simulated this phenology reasonably well, whereas the single *Amax* version underestimated the spring increase and did not show the summer decline. These results suggest that variable *Amax* improved the seasonal predictions of NEE by correctly simulating the rapid increase in GPP during the spring (weeks 14 to 20 — April 15 to May 30). Another factor which contributed to the better results with the variable *Amax* version is the optimal temperature curve for the variable *Amax* version which shows that the variable

Table 2 Parameters marked with (#) are fixed and do not vary during optimization. The numbers beside the best parameter set are parameterizations from the runs that were statistically similar ($P = 0.05$) in terms of likelihood. With the first number being the mean and the number after (±) being the standard deviation of the mean

Parameter	Single-*Amax* values	DayCent-Photo values
PS2Mrsp	0.50 (0.48±0.03)	0.44 (0.45±0.02)
Amax	3.63 (3.83±0.34)	3.76 (3.79±0.22)
#*AmaxFrac*	0.76	0.76
#*AmaxScalar*1	1.0	0.0
*AmaxScalar*2	1.0	1.27 (1.27±0.04)
*AmaxScalar*3	1.0	1.17 (1.16±0.04)
*AmaxScalar*4	1.0	0.38 (0.4±0.02)
#*Attenuation*	0.5	0.5
BaseFolRespFrac	0.100 (0.112±0.021)	0.055 (0.095±0.027)
CFracLeaf	0.56 (0.58±0.04)	0.59 (0.62±0.03)
#*DVPDExp*	−0.35	−0.35
#*DVPDSlope*	1.55	1.55
#*GrowthDays*1	1	1
*GrowthDays*2	1	44 (44±0.48)
*GrowthDays*3	1	135 (135±1.22)
*GrowthDays*4	1	211 (210±2.00)
HalfSatPAR	4.02 (4.21±0.19)	4.25 (4.25±0.14)
#*LeafCSPWT*	270.0	270.0
PsntMin	−1.51 (−1.69±0.54)	−6.67 (−6.23±0.60)
PsntOpt	15.68 (15.85±0.28)	11.67 (11.68±0.14)

Table 3 Model comparison for DayCent model. Single-*Amax* is the photosynthetic version of DayCent with a single *Amax* value. DayCent-Photo is the photosynthetic model with seasonal variation of *Amax*. Root Mean Square Error (RMSE) is a measure of the amount of variance not explained by the model, lower is better. Akaike Information Criterion (AIC) equation is $2K - 2\ln(L)$, where $\ln(L) = Ltotal$. A lower AIC indicates the model that has better support from the data

DayCent Model	Single-*Amax*	DayCent-Photo
Log-likelihood (*Ltotal*)	−1850.0	−1029.5
NEE RMSE/(gC·m^{-2})	0.74	0.63
NEE R^2	0.57	0.69
GPP RMSE/(gC·m^{-2})	1.02	0.88
GPP R^2	0.78	0.84
Number of parameters (*K*)	12	20
AIC	3723.9	2099.0

Amax version temperature curve starts much earlier and at a higher scalar value (not shown). The net effect on GPP is a quicker and larger response to early season temperature increases for the variable *Amax* version.

3.3 DayCent-Photo model validation

Model validation was done with GPP and NEE data withheld from the optimization period from 2006 to 2008, except estimates of GPP were not available for 2008. Validation runs for the DayCent-Photo model were done using the best parameter set from the optimization process. A comparison for the optimization and validation period showed similar R^2 values for GPP and NEE estimates. The similar NEE and GPP results obtained (Fig. 4) for the optimization and validation period strongly support the

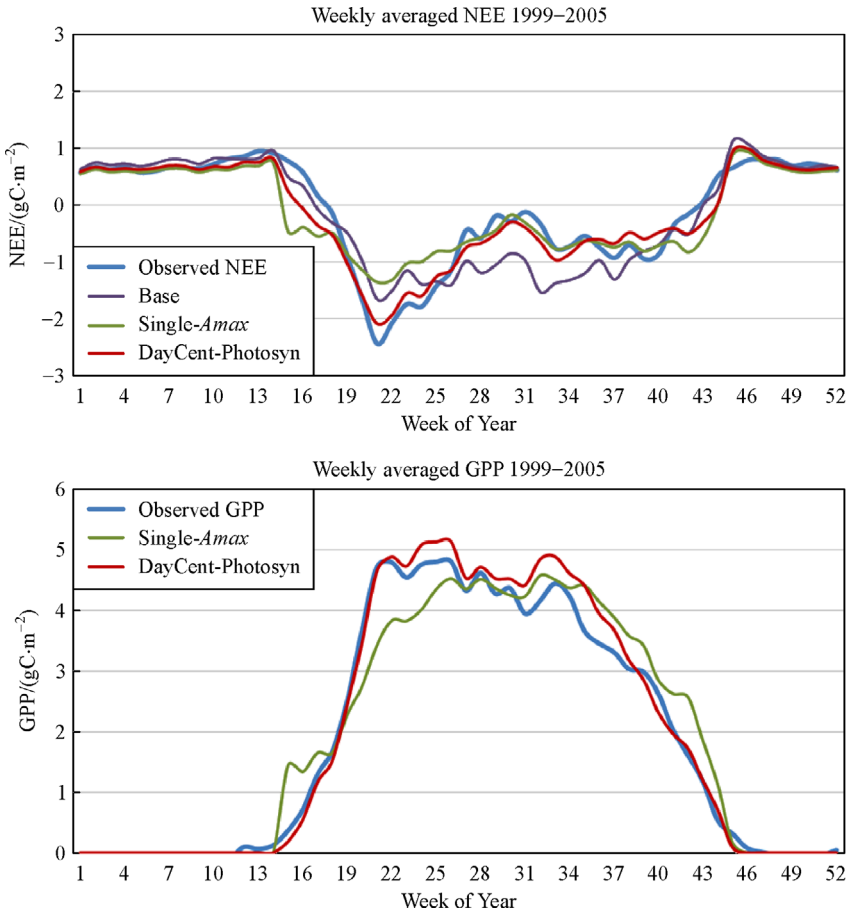

Fig. 3 Model comparison of GPP and NEE for the optimization period from 1999–2005. The data is averaged into 52 weekly periods. Note there is no GPP data for the Base DayCent model because the Base DayCent model where DayCent-Photo is developed from does not have the specialized module for GPP calculation.

addition of not only the photosynthetic sub-model, but also the inclusion of the seasonally variable *Amax*.

Figure 5 shows the comparison of observed vs. simulated daily NEE, GPP, and RESP for the Niwot Ridge site for 2005 using the variable *Amax* version of DayCent-Photo. The results for GPP and RESP (Fig. 5) show that the model simulated observed daily value quite well (model vs. observed data $R^2 > 0.88$). The model simulated correct seasonal pattern in GPP with maximum values of GPP in the spring, rapid increases in GPP from April to May, and rapid decreases in GPP during the September to October time period. The model and observed results for ecosystem respiration (RESP) show that the peak value occurred during the middle of the summer with low values during the winter months. The RESP results generally followed the seasonal pattern of air temperature with maximum RESP and air temperatures (TEMP) during the middle of the summer, increasing RESP and TEMP during the spring, decreasing values during the fall and low values during winter months (temperature data not shown). Both the model results and observed 2005 NEE show that peak carbon uptake occurred in the spring (May), net carbon losses during the winter, and a short period of net carbon uptake in July and August. An inter-annual comparison of NEE for the variable and fix *Amax* versions of Daycent show the differences season responses of each model, with Fig. 6 show three consecutive years of simulations.

Comparison of cumulative annual average NEE show an average net uptake of carbon of 36.0 $gC \cdot m^{-2}$ for the observed data and 40.0 $gC \cdot m^{-2}$ for the model results. The results show that R^2 of the model vs observed for NEE and AET are lower than R^2 for GPP and RESP ($R^2 > 0.88$ for GPP and RESP and R^2 of 0.66 and 0.67 for NEE and AET).

4 Discussion

Our results justify incorporating a photosynthetic sub-model and variable *Amax* into the DayCent model. The resulting DayCent-Photo simulated NEE, GPP, and ecosystem respiration (RESP) much better than the Base and the single *Amax* versions even after penalizing the

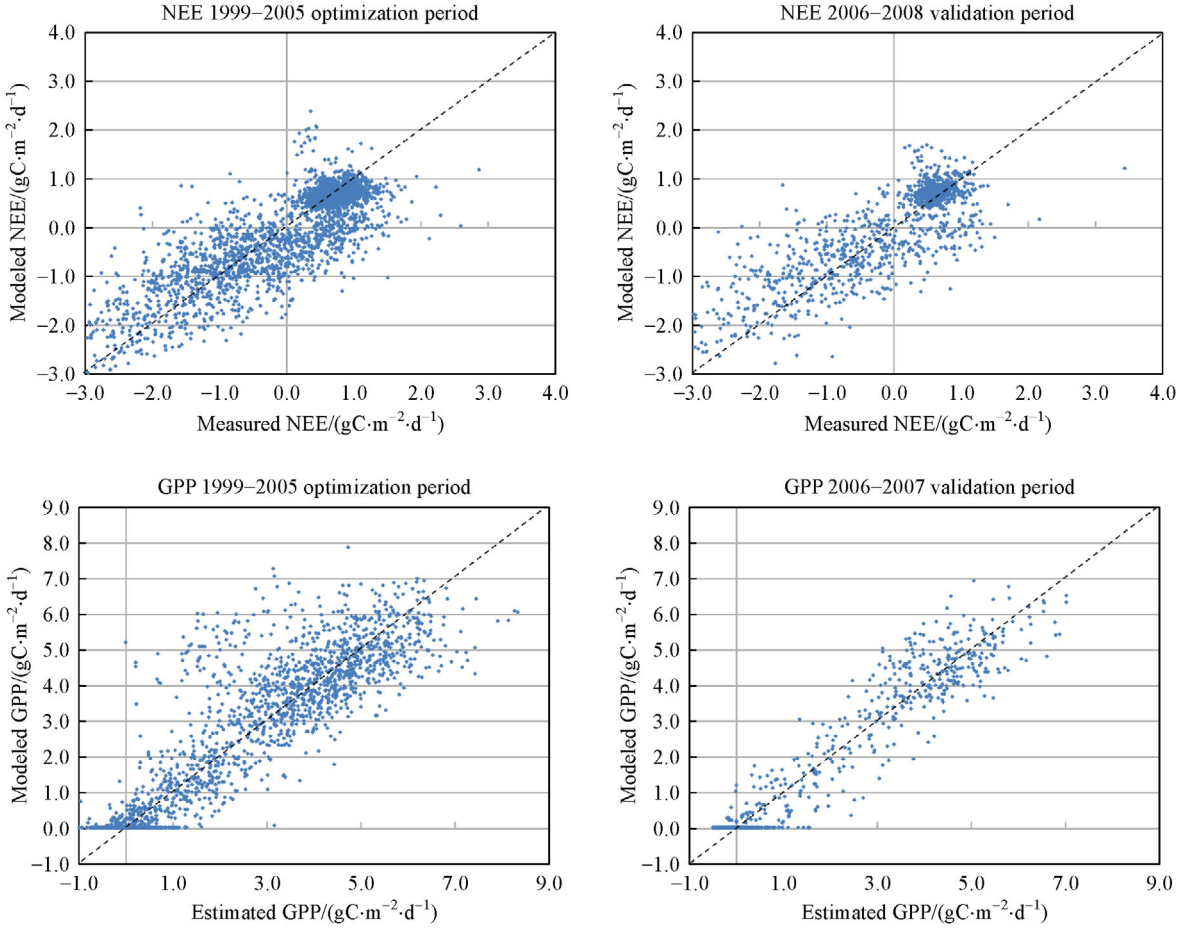

Fig. 4 Model versus data comparisons for the optimization period 1999–2005 and validation period 2006–2008. GPP data is not available for 2008. Positive NEE number denotes release of carbon from the ecosystem to the atmosphere. The large number of data points above one-to-one line for the GPP optimization period is a result of an unexplained large drop in summer time GPP from the observed data in the summer of 2004. If this data is removed, there is a much better correlation (R^2 = 0.91) with the validation period GPP.

model for including extra parameters. The results suggest that seasonality of GPP can be simulated by varying the capacity of canopy level photosynthesis. The biology behind the seasonality of GPP is certainly more complex than the variable *Amax* function we used, but the varying *Amax* maybe adequate enough to capture some aspects of the variability. The variable photosynthetic capacity has four known factors: 1) lower carbon uptake at the start of the growing season due to slow recovery of stomatal conductance (Monson et al., 2005); 2) reduced carbon uptake due to increased temperature at mid-summer (Huxman et al., 2003); 3) differences in assimilation rates of young versus old needles as canopy turns over during the growing season (Mohren and van de Veen, 1995; Marshall et al., 2001; McGarvey et al., 2004; Weiskittel et al., 2006); and 4) an increase in leaf area index (Wang and Barrett, 2003) resulting from needle growth during the growing season. The first and second factors are likely related to stomatal response to water availability, and the third and fourth factors may be related to the distribution of leaves within the layers of the canopy. The photosynthesis sub-model of DayCent-Photo is simple, with one-layer canopy and lumped parameter photosynthesis lacking stomatal conductance. This simplicity may have resulted in the single *Amax* version to poorly simulate the seasonality of GPP, but the simplicity was adequately augmented by the addition of the variable *Amax* function.

The model simulated NEE and especially GPP well across six years (Fig. 3), and likely can simulate them well for the near future given that climate change may shift the the beginning of seaonal growth by a few days per decade. For sub-alpine forests, how the seasonality will shift remains uncertain (Richardson et al., 2013), but the timing of tree flowering has advanced by 1 to 5 days per decade (Ziello et al., 2009). In boreal forests, spring leaf out has advanced by 0.3–1.1 days per decade in Norway (Linkosalo et al., 2009), and by 6.3 days per decade

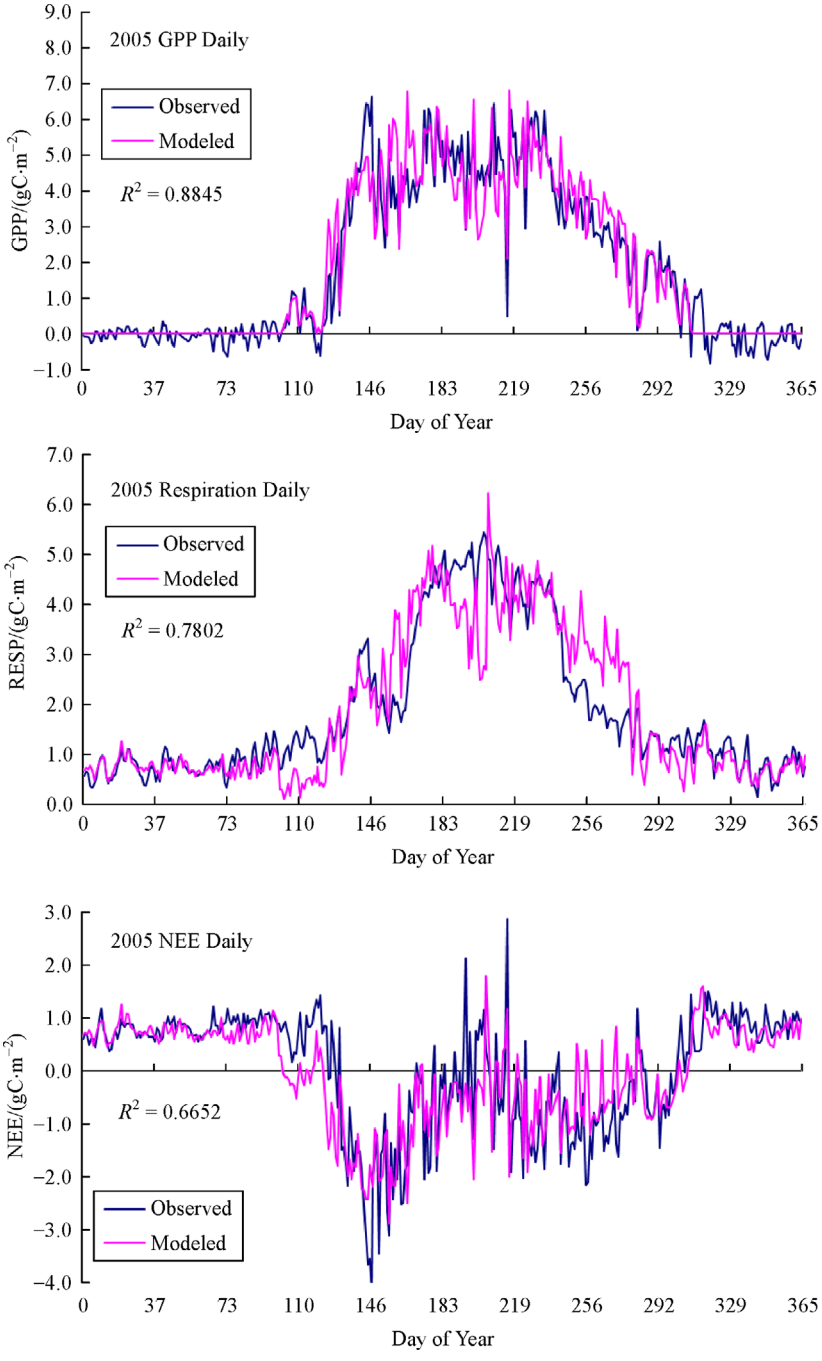

Fig. 5 Comparison of model vs. observed daily GPP (a), RESP (b), and NEE (c) for 2005 at the Niwot Ridge site.

elsewhere in Europe (Delbart et al., 2008). The model is able to simulate the advancing spring leaf out if the advancement is controlled by temperature. Leaf out and start of spring photosynthesis is a function of temperature in DayCent-Photo. The variable *Amax* function cannot predict how climate change affects the phenology of photosynthesis, but the phenology likely will change gradually for the near future, gradual enough for DayCent-Photo to predict NEE reasonably well. Seasonality of NEE may be due to temperature acclimation of photosynthesis, with colder sites slower to acclimate (Gea-Izquierdo et al., 2010), suggesting that the optimization and validation should be site specific.

This study focused on the photosynthesis sub-model of DayCent, and the sub-model represents only a small portion of the total ecosystem processes that are simulated by the DayCent model. Since there are many papers that describe the setup and running of the DayCent model (Paustian et al., 1992; Parton and Rasmussen, 1994; Parton et al., 1998), we limited our variability and analysis to only

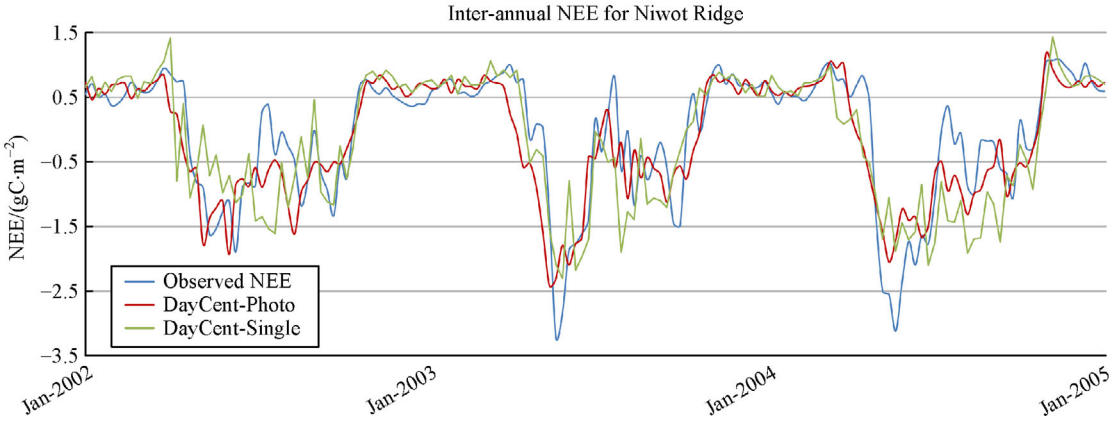

Fig. 6 Comparison of Inter-annual NEE for Niwot Ridge for the DayCent with fixed (DayCent-Single) and variable (DayCent-Photo) vs. observed NEE.

the new parameters added in the sub-model. The model performance could be further improved by adjusting other parameters, such as those controlling autotrophic and heterotrophic respiration rates. The DayCent-Photo model slightly overestimated NEE (more carbon uptake than observed, Fig. 3), as a result of overestimating GPP during the summer period and underestimating RESP in the onset and end of growing season. Climate change can hasten the date the forest transitions from carbon sink to source in autumn, primarily from increased RESP (Piao et al., 2008), and more accurate simulation of RESP may be critical in predicting the carbon dynamics of the forest in the future.

The errors in NEE reported here do not include errors in the data. The eddy covariance technique typically underestimates RESP compared chamber-based measurements due to the influence of effects such as drainage and advection (Massman and Lee, 2002). Speckman et al. (2015) showed that even with high wind speed RESP derived from the nighttime eddy covariance measurements was underestimated in a nearby forest in Wyoming. The errors associated with eddy covariance technique are estimated to be $30-100\ gC\cdot m^{-2}\cdot y^{-1}$ (Baldocchi, 2008), and while DayCent-Photo overestimated the annual sum by less than $10\ gC\cdot m^{-2}$.

The DayCent-Photo model has recently been used to successfully simulate seasonal patterns in AET, NEE, GPP and RESP for deciduous forest, conifer forest, and grassland (Savage et al., 2013; Chen et al., 2016). The results from all of these papers suggest that *Amax* has a similar seasonal patterns for grasslands and forest systems with *Amax* values being highest in the May to early June time period and low during the spring and fall months. The results show that including variable *Amax* greatly improved the ability of the model to simulate seasonal patterns in ecosystem variables and that observed seasonal patterns in GPP and NEE from the AmeriFlux sites can be used to successfully parameterize the seasonal changes in *Amax*. The recent results show that the DayCent-Photo model can be used to simulate ecosystem dynamics for different biomes (grasslands, conifer forests, and deciduous forest). We are currently expanding the use of the DayCent-Photo model to simulate seasonal changes in AET, NEE, GPP, and RESP for all of the major biomes (savanna, tell grass prairie and other forest types) in the world using data sets from AmeriFlux sites.

5 Conclusions

For this study we modified the DayCent model to include a photosynthetic sub-model with seasonally variable photosynthetic capacity. Compared to the base DayCent and single *Amax* versions, the inclusion of the photosynthesis sub-model and variable *Amax* was strongly supported by observations, even after the extra parameters were penalized for extra degrees of freedom. These results suggest that the seasonality of GPP and NEE in this system arises from the changes in photosynthetic capacity. The biological process behind the seasonality likely involves the complex biology of stomatal conductance, drought response, and leaf turnover.

By modeling the seasonal variation in the NEE flux through model optimization procedure, we extracted information about the necessary model structure needed to simulate the seasonality of photosynthesis. Extrapolating model structure to a biological process equation will be the next significant step in understanding the effect of *Amax* for different ecosystems. Once this is in place we can gain a further understanding the on the role variable *Amax* plays on ecosystems under various levels of stress. DayCent-Photo has been successfully used to simulate seasonal changes in ecosystem variables for grassland and forest ecosystems using AmeriFlux data sets to calibrate and test the model and has the potential to be successfully used to simulate ecosystem dynamics for all of the major ecosystems in the world.

Acknowledgements This work is supported by the US Department of Agriculture (USDA) UV-B Monitoring and Research Program, Colorado State University, under USDA National Institute of Food and Agriculture Grant 2016-34263-25763.

References

Aber J D, Federer C A (1992). A generalized, lumped-parameter model of photosynthesis, evapotranspiration and net primary production in temperate and boreal forest ecosystems. Oecologia, 92(4): 463–474

Baldocchi D D (2008). Breathing of the terrestrial biosphere: lessons learned from a global network of carbon dioxide flux measurement systems. Aust J Bot, 56(1): 1–26

Baldocchi D D (2003). Assessing the eddy covariance technique for evaluating carbon dioxide exchange rates of ecosystems: past, present and future. Glob Change Biol, 9(4): 479–492

Baldocchi D D, Hincks B B, Meyers T P (1988). Measuring biosphere-atmosphere exchanges of biologically related gases with micro-meteorological methods. Ecology, 69(5): 1331–1340

Blanken P D, Monson R K, Burns S P, Turnipseed A A (2010). Data and Information for the US-NR1 Niwot Ridge Subalpine Forest AmeriFlux Site (LTER NWT1). AmeriFlux Management Project. Lawrence Berkeley National Laboratory, California

Bourdeau P F (1959). Seasonal variations of the photosynthetic efficiency of evergreen conifers. Ecology, 40(1): 63–67

Braswell B H, Sacks W J, Linder E, Schimel D S (2005). Estimating diurnal to annual ecosystem parameters by synthesis of a carbon flux model with eddy covariance net ecosystem exchange observations. Glob Change Biol, 11(2): 335–355

Chen M, Parton W J, Adair E C, Asao S, Hartman M D, Gao W (2016). Simulation of the effects of photodecay on long-term litter decay using DayCent. Ecosphere, 7(12): e01631

Chen M, Parton W J, Del Grosso S J, Hartman M D, Day K A, Tucker C J, Derner J D, Knapp A K, Smith W K, Ojima D S, Gao W (2017). The signature of sea surface temperature anomalies on the dynamics of semiarid grassland productivity. Ecosphere, 8(12): e02069

Del Grosso S J, Parton W J, Mosier A R, Hartman M D, Brenner J, Ojima D S, Schimel D S (2001). Simulated Interaction of Carbon Dynamics and Nitrogen Trace Gas Fluxes Using the DAYCENT Model. In: Shaffer M J, Ma L W, Hansen S, eds. Modeling Carbon and Nitrogen Dynamics for Soil Management. Boca Raton: CRC Press, 303–332

Del Grosso S J, Parton W J, Mosier A R, Ojima D S, Kulmala A E, Phongpan S (2000). General model for N_2O and N_2 gas emissions from soils due to dentrification. Global Biogeochem Cycles, 14(4): 1045–1060

Del Grosso S J, Parton W J, Stohlgren T J, Zheng D L, Bachelet D, Prince S, Hibbard K, Olson R (2008). Global potential net primary production predicted from vegetation class, precipitation, and temperature. Ecology, 89(8): 2117–2126

Delbart N, Picard G, Le Toan T, Kergoat L, Quegan S, Woodward I, Dye D, Fedotova V (2008). Spring phenology in boreal Eurasia over a nearly century time scale. Glob Change Biol, 14(3): 603–614

Drake J E, Raetz L M, Davis S C, Delucia E H (2010). Hydraulic limitation not declining nitrogen availability causes the age-related photosynthetic decline in loblolly pine (*Pinus taeda* L.). Plant Cell Environ, 33(10): 1756–1766

Fisher R A (1932). Inverse probability and the use of likelihood. Math Proc Camb Philos Soc, 28(03): 257–261

Frey S D, Lee J, Melillo J M, Six J (2013). The temperature response of soil microbial efficiency and its feedback to climate. Nat Clim Chang, 3(4): 395–398

Gea-Izquierdo G, Mäkelä A, Margolis H, Bergeron Y, Black T A, Dunn A, Hadley J, Paw U K T, Falk M, Wharton S, Monson R, Hollinger D Y, Laurila T, Aurela M, McCaughey H, Bourque C, Vesala T, Berninger F (2010). Modeling acclimation of photosynthesis to temperature in evergreen conifer forests. New Phytol, 188(1): 175–186

Granda E, Scoffoni C, Rubio-Casal A E, Sack L, Valladares F (2014). Leaf and stem physiological responses to summer and winter extremes of woody species across temperate ecosystems. Oikos, 123 (11): 1281–1290

Guan M, Jin Z, Wang Q, Li Y, Zuo W (2014). Response of photosynthesis traits of dominant plant species to different light regimes in the secondary forest in the area of Qiandao Lake, Zhejiang, China. China Journal of Applied Ecology, 25: 1615–1622

Hartman M D, Baron J S, Ewing H A, Weathers K C (2014). Combined global change effects on ecosystem processes in nine U.S. topographically complex areas. Biogeochemistry, 119(1 – 3): 85–108

Helms J A (1965). Diurnal and seasonal patterns of net assimilation in Douglas-Fir, *Pseudotsuga Menziesii* (Mirb). Franco, as Influenced by Environment. Ecology, 46(5): 698–708

Hilborn R, Mangel M (1997). The ecological detective: confronting models with data. Monogr Popul Biol, 28: 315

Hurtt G C, Armstrong R (1996). A pelagic ecosystem model calibrated with BATS data. Deep Sea Res Part II Top Stud Oceanogr, 43(2 – 3): 653–683

Huxman T E, Turnipseed A A, Sparks J P, Harley P C, Monson R K (2003). Temperature as a control over ecosystem CO_2 fluxes in a high-elevation, subalpine forest. Oecologia, 134(4): 537–546

Johnson J B, Omland K S (2004). Model selection in ecology and evolution. Trends Ecol Evol, 19(2): 101–108

Kelly R H, Parton W J, Hartman M D, Stretch L K, Ojima D S, Schimel D S (2000). Intra-annual and interannual variability of ecosystem processes in shortgrass steppe. Journal of Geophysical Research: Atmospheres, 105(D15): 20093–20100

Li Z, Li X, Rubert-Nason K F, Yang Q, Fu Q, Feng J, Shi S (2018). Photosynthetic acclimation of an evergreen broadleaved shrub (*Ammopiptanthus mongolicus*) to seasonal climate extremes on the Alxa Plateau, a cold desert ecosystem. Trees (Berl), 32(2): 603–614

Linkosalo T, Häkkinen R, Terhivuo J, Tuomenvirta H, Hari P (2009). The time series of flowering and leaf bud burst of boreal trees (1846-2005) support the direct temperature observations of climatic warming. Agric Meteorol, 149(3–4): 453–461

Luyssaert S, Ciais P, Piao S L, Schulze E D, Jung M, Zaehle S, Schelhaas M J, Reichstein M, Churkina G, Papale D, Abril G, Beer C, Grace J, Loustau D, Matteucci G, Magnani F, Nabuurs G J, Verbeeck H, Sulkava M, van der WERF G R, Janssens I A (2010). The European carbon balance. Part 3: forests. Glob Change Biol, 16 (5): 1429–1450

Luyssaert S, Schulze E D, Börner A, Knohl A, Hessenmöller D, Law B E, Ciais P, Grace J (2008). Old-growth forests as global carbon sinks.

Nature, 455(7210): 213–215

Marshall J D, Rehfeldt G E, Monserud R A (2001). Family differences in height growth and photosynthetic traits in three conifers. Tree Physiol, 21(11): 727–734

Martinez K A, Fridley J D (2018). Acclimation of leaf traits in seasonal light environments: Are non-native species more plastic? J Ecol, 20: 207–216

Massman W J, Lee X (2002). Eddy covariance flux corrections and uncertainties in long-term studies of carbon and energy exchanges. Agric Meteorol, 113(1 – 4): 121–144

McGarvey R C, Martin T A, White T L (2004). Integrating within-crown variation in net photosynthesis in loblolly and slash pine families. Tree Physiol, 24(11): 1209–1220

Mohren G M J, van de Veen J R (1995). Forest growth in relation to site conditions. Application of the model forgro to the Solling spruce site. Ecol Modell, 83(1 – 2): 173–183

Monson R K, Sparks J P, Rosenstiel T N, Scott-Denton L E, Huxman T E, Harley P C, Turnipseed A A, Burns S P, Backlund B, Hu J (2005). Climatic influences on net ecosystem CO_2 exchange during the transition from wintertime carbon source to springtime carbon sink in a high-elevation, subalpine forest. Oecologia, 146(1): 130–147

Monson R K, Turnipseed A A, Sparks J P, Harley P C, Scott-Denton L E, Sparks K, Huxman T E (2002). Carbon sequestration in a high-elevation, subalpine forest. Glob Change Biol, 8(5): 459–478

Moore D J P, Hu J, Sacks W J, Schimel D S, Monson R K (2008). Estimating transpiration and the sensitivity of carbon uptake to water availability in a subalpine forest using a simple ecosystem process model informed by measured net CO_2 and H_2O fluxes. Agric Meteorol, 148(10): 1467–1477

Papale D, Valentini R (2003). A new assessment of European forests carbon exchanges by eddy fluxes and artificial neural network spatialization. Glob Change Biol, 9(4): 525–535

Parton W J, Hanson P J, Swanston C, Torn M, Trumbore S E, Riley W, Kelly R (2010). ForCent model development and testing using the enriched background isotope study experiment. J Geophys Res, 115 (G4): G04001

Parton W J, Hartman M, Ojima D, Schimel D (1998). DAYCENT and its land surface submodel: description and testing. Global Planet Change, 19(1 – 4): 35–48

Parton W J, Rasmussen P E (1994). Long-term effects of crop management in wheat/fallow: II. CENTURY model simulations. Soil Sci Soc Am J, 58(2): 530–536

Parton W, Holland E A, Del Grosso S J, Hartman D, Martin M, Mosier A, Ojima D S, Schimel D S (2001). Generalized model for NO_x and N_2O emissions from soils. J Geophys Res, 106(D15): 17403–17419

Paustian K, Parton W J, Persson J (1992). Modeling soil organic matter in organic-amended and nitrogen-fertilized long-term plots. Soil Sci Soc Am J, 56(2): 476–488

Piao S, Ciais P, Friedlingstein P, Peylin P, Reichstein M, Luyssaert S, Margolis H, Fang J, Barr A, Chen A, Grelle A, Hollinger D Y, Laurila T, Lindroth A, Richardson A D, Vesala T (2008). Net carbon dioxide losses of northern ecosystems in response to autumn warming. Nature, 451(7174): 49–52

Rastetter E B, Aber J D, Peters D P C, Ojima D S, Burke I C (2003). Using mechanistic models to scale ecological processes across space and time. Bioscience, 53(1): 68

Reichstein M, Falge E, Baldocchi D, Papale D, Aubinet M, Berbigier P, Bernhofer C, Buchmann N, Gilmanov T, Granier A, Grunwald T, Havrankova K, Ilvesniemi H, Janous D, Knohl A, Laurila T, Lohila A, Loustau D, Matteucci G, Meyers T, Miglietta F, Ourcival J M, Pumpanen J, Rambal S, Rotenberg E, Sanz M, Tenhunen J, Seufert G, Vaccari F, Vesala T, Yakir D, Valentini R (2005). On the separation of net ecosystem exchange into assimilation and ecosystem respiration: review and improved algorithm. Glob Change Biol, 11(9): 1424–1439

Richardson A D, Keenan T F, Migliavacca M, Ryu Y, Sonnentag O, Toomey M (2013). Climate change, phenology, and phenological control of vegetation feedbacks to the climate system. Agric Meteorol, 169: 156–173

Ryan M G, Waring R H (1992). Maintenance respiration and stand development in a young subalpine lodgepole pine forest. Ecology, 73: 2100–2108

Sacks W J, Schimel D S, Monson R K (2007). Coupling between carbon cycling and climate in a high-elevation, subalpine forest: a model-data fusion analysis. Oecologia, 151(1): 54–68

Sacks W J, Schimel D S, Monson R K, Braswell B H (2006). Model-data synthesis of diurnal and seasonal CO_2 fluxes at Niwot Ridge, Colorado. Glob Change Biol, 12(2): 240–259

Savage K E, Parton W J, Davidson E A, Trumbore S E, Frey S D (2013). Long-term changes in forest carbon under temperature and nitrogen amendments in a temperate northern hardwood forest. Glob Change Biol, 19(8): 2389–2400

Schimel D (1995). Terrestrial ecosystems and the carbon cycle. Glob Change Biol, 1(1): 77–91

Speckman H N, Frank J M, Bradford J B, Miles B L, Massman W J, Parton W J, Ryan M G (2015). Forest ecosystem respiration estimated from eddy covariance and chamber measurements under high turbulence and substantial tree mortality from bark beetles. Glob Change Biol, 21(2): 708–721

Tang X, Wang X, Wang Z, Liu D, Jia M, Dong Z, Xie J, Ding Z, Wang H, Liu X (2013). Influence of vegetation phenology on modelling carbon fluxes in temperate deciduous forest by exclusive use of MODIS time-series data. Int J Remote Sens, 34(23): 8373–8392

Tang X, Wang Z, Liu D, Song K, Jia M, Dong Z, Munger J W, Hollinger D Y, Bolstad P V, Goldstein A H, Desai A R, Dragoni D, Liu X (2012). Estimating the net ecosystem exchange for the major forests in the northern United States by integrating MODIS and AmeriFlux data. Agric Meteorol, 156: 75–84

Turnipseed A A, Anderson D E, Blanken P D, Baugh W M, Monson R K (2003). Airflows and turbulent flux measurements in mountainous terrain. Part 1. Canopy and local effects. Agric Meteorol, 119(1 – 2): 1–21

Turnipseed A A, Anderson D E, Burns S, Blanken P D, Monson R K (2004). Airflows and turbulent flux measurements in mountainous terrain: Part 2: Mesoscale effects. Agric Meteorol, 125(3 – 4): 187–205

Turnipseed A A, Blanken P D, Anderson D E, Monson R K (2002). Energy budget above a high-elevation subalpine forest in complex topography. Agric Meteorol, 110(3): 177–201

Urban O, Holub P, Klem K (2017). Seasonal courses of photosynthetic parameters in sun- and shade-acclimated spruce shoots. Beskydy, 10 (1 – 2): 49–56

Wang Y P, Baldocchi D, Leuning R, Falge E, Vesala T (2007). Estimating parameters in a land-surface model by applying nonlinear inversion to eddy covariance flux measurements from eight FLUXNET sites. Glob Change Biol, 13(3): 652–670

Wang Y P, Barrett D J (2003). Estimating regional terrestrial carbon fluxes for the Australian continent using a multiple-constraint approach I. Using remotely sensed data and ecological observations of net primary production. Tellus B Chem Phys Meterol, 55: 270–289

Weiskittel A R, Maguire D, Garber S M, Kanaskie A (2006). Influence of Swiss needle cast on foliage age-class structure and vertical foliage distribution in Douglas-fir plantations in north coastal Oregon. Can J Res, 36(6): 1497–1508

Zhang Y J, Holbrook N M, Cao K F (2014). Seasonal dynamics in photosynthesis of woody plants at the northern limit of Asian tropics: potential role of fog in maintaining tropical rainforests and agriculture in Southwest China. Tree Physiol, 34(10): 1069–1078

Zhang Y J, Sack L, Cao K F, Wei X M, Li N (2017). Speed versus endurance tradeoff in plants: leaves with higher photosynthetic rates show stronger seasonal declines. Sci Rep, 7(1): 42085

Ziello C, Estrella N, Kostova M, Koch E, Menzel A (2009). Influence of altitude on phenology of selected plant species in the Alpine region (1971-2000). Clim Res, 39: 227–234

Zobitz J M, Moore D J P, Sacks W J, Monson R K, Bowling D R, Schimel D S (2008). Integration of process-based soil respiration models with whole-ecosystem CO_2 measurements. Ecosystems (N Y), 11(2): 250–269